Concentric Eye Walls, Secondary Wind Maxima, and The Evolution of the Hurricane Vortex

H. E. WILLOUGHBY, J. A. CLOS[1] AND M. G. SHOREIBAH[2]

NHRL/AOML/NOAA, Coral Gables, FL 33146

(Manuscript received 20 July 1981, in final form 13 October 1981)

ABSTRACT

Research aircraft observations in recent hurricanes support the model of Shapiro and Willoughby (1982) for the tropical cyclone's response to circularly symmetric, convective heat sources (convective rings). In both nature and the numerical model the tangential wind commonly increases rapidly just inside the radius of maximum wind and decreases inside the eye near the central axis of the vortex. Thus both secondary outer wind maxima and eyewall wind maxima often contract as they intensify. This response is independent of the horizontal spatial scale of the maximum. An outer maximum is frequently observed to constrict about a pre-existing eye and replace it. This chain of events often coincides with a weakening, or at least a pause in intensification, of the vortex as a whole. The concentric eye phenomenon is a common, but by no means universal, feature of tropical cyclones. It is most frequently observed in intense, highly symmetric systems.

1. Introduction

Shapiro and Willoughby (1982, this issue, hereafter referred to as SW) applied Eliassen's (1951) model of forced secondary circulations to tropical cyclones. This model diagnosed the transverse flow induced by point sources of heat or momentum in balanced, axisymmetric vortices. Scale analysis revealed that the nondimensional response to a fixed source was independent of the vortex's horizontal scale. For either a heat or a momentum source near a maximum of the tangential wind, the height of standard isobaric surfaces fell rapidly inside the radius of maximum wind and much more slowly outside it. The sharpest gradient of isobaric height fall lay just inside the wind maximum and supported a sharp peak of the tangential wind tendency. Because this peak lay inside the maximum of the wind itself, the maximum propagated inward in response to heating. This aspect of the model provides a plausible explanation for the observed contraction of the eye in intensifying hurricanes. A heat source isolated from the wind maximum accelerated the tangential wind at and inside the radius of the source. This led to formation of a secondary wind maximum. In either case the winds commonly decreased near the central axis of the vortex. The nondimensional horizontal scale of the response depended strongly upon the maximum wind speed. For a stronger vortex, the response was more localized near the source and more efficient in intensifying the vortex.

This dynamic model was formulated in terms of specified point sources in the radius–height plane. In the axisymmetric context of the model, such sources are really rings of heating. We coin the term "convective ring" for the SW formulation. The present study is directed toward interpretation of aircraft observations of the evolution of eye walls and secondary wind maxima in terms of the convective ring model. These convective rings are prevalent in strong, axisymmetric tropical cyclones. As we shall see below, they are not observed in tropical storms or weak hurricanes and typhoons. Highly asymmetric, less intense hurricanes appear to be dominated by spiral-shaped wind and radar reflectivity features rather than rings. In 1979 Hurricanes Frederic, throughout its development, and David, after its passage over the Greater Antilles, were notable examples of asymmetric systems that did not form outer convective rings.

Observationally, secondary wind maxima and concentric eyes occur in hurricanes when a second ring of active convection forms around a pre-existing eyewall. The outer eye often contracts and intensifies as the inner eye weakens and eventually vanishes. The destruction of the inner eye usually marks the end of an episode of falling central surface pressure.

This concentric eye cycle has been described by a number of previous workers. Fortner (1958) was first to describe this phenomenon. In Typhoon Sarah of 1956, reconnaissance aircraft observed 90 m s^{-1}

[1] Present affiliation: Bell Telephone Laboratories, Denver, CO 80234.

[2] Present address: Prescott Hall, University of Michigan, Ann Arbor, 48109.

winds and 94 kPa central pressure at a time when the typhoon had an inner eye of 6 km diameter surrounded by a 28 km outer eye. Eight hours later the inner eye had disappeared, the outer eye had contracted to 16 km, and the maximum wind had decreased to 44 m s^{-1}.

Jordan and Schatzle (1961) and Jordan (1966) reported concentric eyes in Hurricanes Donna of 1960 and Carla of 1961, but did not relate them to intensity fluctuations. Hoose and Colón (1970) documented a complete concentric eye cycle during 36 h of continuous radar observation in Hurricane Beulah of 1967. Initially the outer eye was 67 km in diameter and the inner eye 11 km. Over a period of 13 h the outer eye contracted to 30 km, while the inner eye deteriorated and vanished. The wind maximum shifted to the outer eyewall as the inner eye faded. As the outer maximum replaced the inner, the central pressure attained a minimum value of 94 kPa and subsequently rose.

Holliday (1977) described similar behavior in Typhoon Gloria of 1974. In this case, the initial diameters of the outer and inner eyes were 56 and 7.5 km. The outer eye contracted to 37 km diameter and the inner disappeared in 11.5 h. In the same interval the central pressure rose from 93.7 to 95.5 kPa.

During the STORMFURY modification experiment, on 20 August 1969, a concentric eye wall associated with a secondary wind maximum was observed in Hurricane Debbie (Gentry, 1970; Hawkins, 1971; Black *et al.*, 1972). As in the unmodified cases, the maximum wind decreased and appeared farther from the center. Whether this was a consequence of human intervention or a manifestation of a natural concentric eye cycle remains controversial.

In the next section, we present observations from Hurricanes Anita of 1977 and David of 1979. We first attempt to track the evolution of wind maxima by fitting linear trend lines to the maximum wind and the radius at which it occurs. This does not lead to satisfactory levels of statistical significance. We then fit linear estimates to the wind and isobaric height at fixed radii with much better results. The estimates allow us to evaluate structure and tendencies that appear to be consistent with the gradient wind relation and the convective ring model. In Section 3 three years' data from Pacific typhoons is examined in an attempt both to verify independently the concentric eye cycle's relation to intensity changes and to evaluate the frequency with which concentric eyes occur. Earlier workers' results, the SW model, and the data in Sections 2 and 3 contribute to the formation of a hypothetical description of convective ring behavior. Multi-aircraft observations from Hurricane Allen of 1980, presented in Section 4, confirm this description in qualitative terms. In Section 5 an attempt is made to use the SW model to simulate observations and to carry out several quantitative checks of the hypothesis. Section 6 contains a summary and interpretation of the results.

2. Hurricanes Anita and David

Hurricane Anita intensified rapidly during the period 30 August–2 September 1977 before making landfall and dissipating on the Mexican coast south of Brownsville, Texas (see Lawrence, 1978). Fig. 1a shows a history of Anita's central pressure and eye diameter. Between 0000 and 0600 GMT 2 September, NOAA-42, one of the Research Facilities Center's (RFC) WP-3D aircraft, operated in the storm and obtained both detailed meteorological measurements and digital radar data. Willoughby (1979c) has prepared a summary of the meteorological data. The aircraft flew at the 70 kPa pressure level and obtained data on a total of 16 radial traverses, 4 along each cardinal compass direction from the center. Fig. 2 illustrates the eight profiles which lie along a north–south axis through the center. While NOAA-42 was in the storm, a secondary wind maximum formed at between 40 and 60 km radius. This feature was most pronounced along the axis illustrated and much weaker, though still present, along the east–west axis. A digital radar composite obtained at the same time as these measurements appears in Fig. 3. The primary eyewall is the ring of 40 dBZ radar returns in the center of the frame. The secondary wind maximum corresponds to the arc of equally intense returns extending from south through east to north at 50–70 km radius from the center. The convective ring was observed as early as 0130 GMT by the land-based WSR-57 radar at Brownsville, then ~150 km from the center (Willoughby, 1979c). Examination of Fig. 1a shows that this happened just after the central pressure fell below 94 kPa. Apparently, the appearance of the convective ring preceded that of the secondary wind maximum. After 0000 GMT 2 September, the rate of intensification slowed, although the approach of landfall may be more important than the effect of the concentric eye. On the whole, this sequence of events resembles the cases of concentric eyes cited in Section 1, but it is less dramatic.

Hurricane David on 30 August 1979 was a much better example of the concentric eye phenomenon. David was a classic Cape Verde tropical cyclone that entered the Caribbean as an intense hurricane (Hebert, 1980). The flight described here was carried out by RFC's C-130B, NOAA-41, as David reached peak intensity. The flight pattern was similar to that flown in Anita, but only 10 radial traverses were obtained. Fig. 4 illustrates six of these along the east–west axis through the center. A secondary wind maximum with winds nearly as strong as those in the eye wall was present between 40 and 60 km radius. In contrast to Anita, David's secondary maximum was

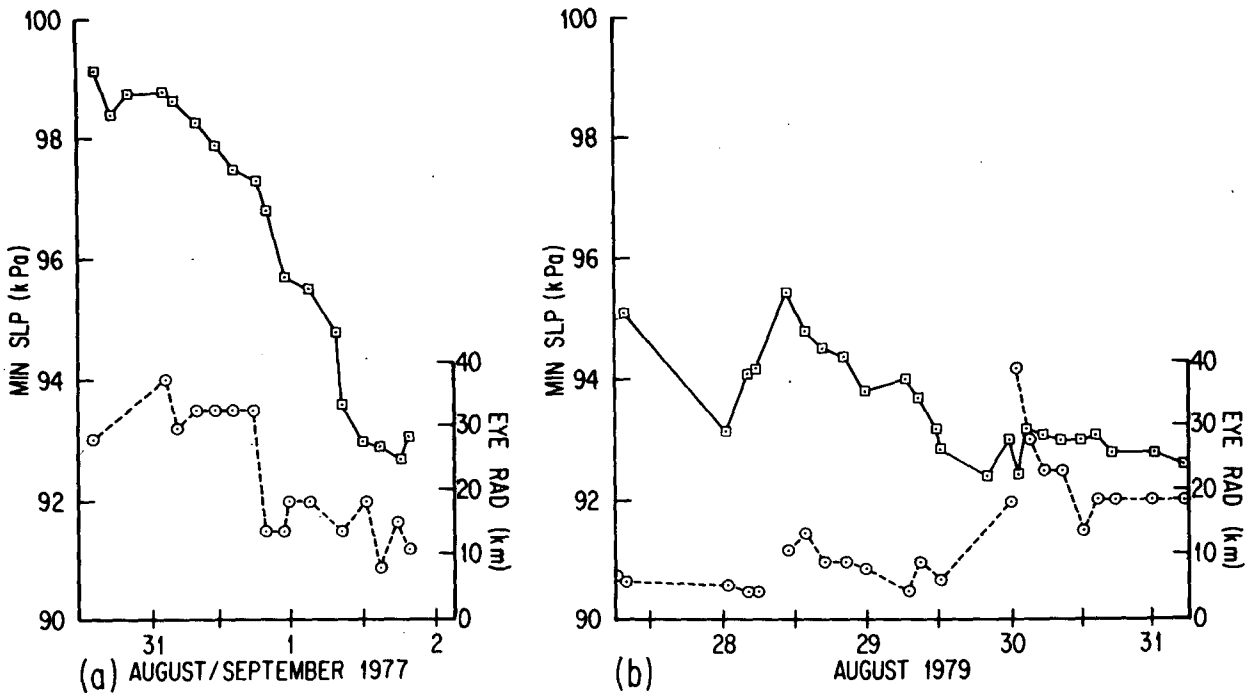

FIG. 1. The evolution of the central pressure (solid lines) and eye radius (dashed lines) in Hurricanes Anita (a) and David (b). The date is plotted at 1200 GMT each day.

symmetric and appeared prominently in all 10 profiles. Although equipment failure prevented acquisition of radar data during NOAA-41's flight, NOAA-43, RFC's second WP-3D, did obtain such data. Fig. 5 shows the prominent concentric eye structure in a digital radar composite for 1045 to 1131 GMT, about an hour after NOAA-41 left the storm. As in Anita, the secondary wind maximum and outer wall cloud coincided. When NOAA-41 returned at 0830 on 31 August only a single eye 24 km in radius was present, and the maximum wind was 10 m s^{-1} more than on 30 August. It seems probable that the inner eye had dissipated and been replaced by the outer convective ring by that time.

Examination of the history of David's central pressure and eye diameter (Fig. 1b) clearly shows the reformation of the eye and increase in central pressure associated with the convective ring on 30 August. This episode marked the end of a deepening trend that had begun 36 h before at 0000 GMT on 29 August. An earlier concentric eye cycle may have marked the beginning of the deepening trend. Between 1800 GMT on 28 August and 0000 GMT on 29 August the eye radius increased by 6 km and the central pressure rose from 93 to 96 kPa. Unfortunately, this earlier cycle was not documented by research aircraft.

In an effort to make the analysis more quantitative we extracted the maximum tangential wind (v_{max}) and the radius at which it occurs (r_{max}) from the profile data. The v_{max} and r_{max} data were least-squares fitted with linear functions of time, regardless of direction from the center. The results of this calculation for Anita appear in Fig. 6. Individual observed values of v_{max} and r_{max} are marked by letters that indicate their direction from the center. The slopes of the regression lines are substantial and consistent with our qualitative impressions from Fig. 2. Application of the two-tailed Student-t test indicates that the slopes are different from zero at the 1% level of significance. The eyewall was thus unambiguously contracting as the maximum wind was increasing.

Other calculations of this kind are less satisfactory. In the case of Anita's secondary maximum it is impossible to choose "the" maximum among several candidates, so that no reliable trend can be established. For David on 30 August both maxima, as well as the minimum between them, are consistently trackable. As Fig. 7 shows, the slopes are consistent with the idea of a contracting, intensifying outer maximum that surrounds a weakening, expanding inner eye. The statistical significance of the slopes, however, is low. A more sensitive means of analysis is required to establish the behavior of the symmetric vortex.

Much of the ambiguity of the foregoing analyses arises from the subjective element introduced by choice of "the" maximum wind. Willoughby's (1979a) scaling analysis shows that the tangential wind and isobaric height data in Figs. 2 and 4 rep-

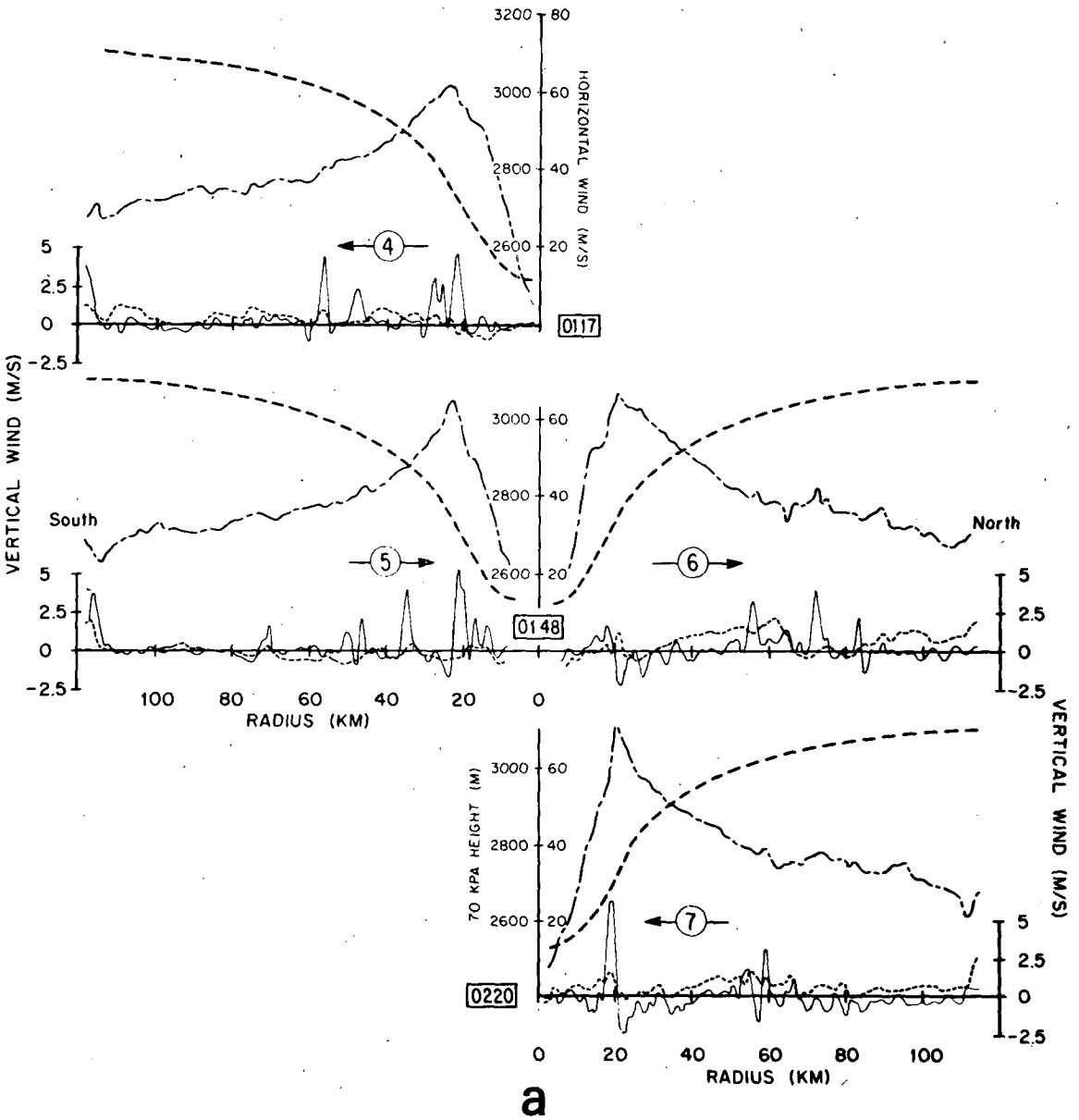

FIG. 2. Radial profiles of meteorological data along a north–south axis in Hurricane Anita on 2 September 1977. The chain-dashed curve is the relative tangential wind, the heavier dashed curve the 70 kPa height, the solid curve the vertical wind, and the lighter dashed curve the relative radial wind. The arrows and numbers in circles indicate direction of flight and traverse number, while the numbers in boxes give the time of passage through the center. Data obtained between (a) 0117 and 0220 GMT and (b) 0334 and 0457.

resent the sum of a slowly evolving symmetric field and a rapidly fluctuating asymmetric one. If a large positive transient lies somewhere other than at the symmetric maximum, it will be interpreted as being "the" maximum even though it is displaced from the symmetric maximum. Thus, both the amplitude and location of the transient peak contribute variability that both distorts the trends and reduces their significance.

This difficulty is overcome if the least-squares algorithm is used to fit the tangential wind and isobaric height fields at fixed radii rather than at the radius of maximum wind. When this is done a transient peak contributes only its amplitude to the rms error and does not distort the apparent location of the maximum.

The original data processing for Figs. 2 and 4 is based on accurate determination of the storm track and interpolation of the meteorological data, including the time of observation, onto a 0.5 km radial grid

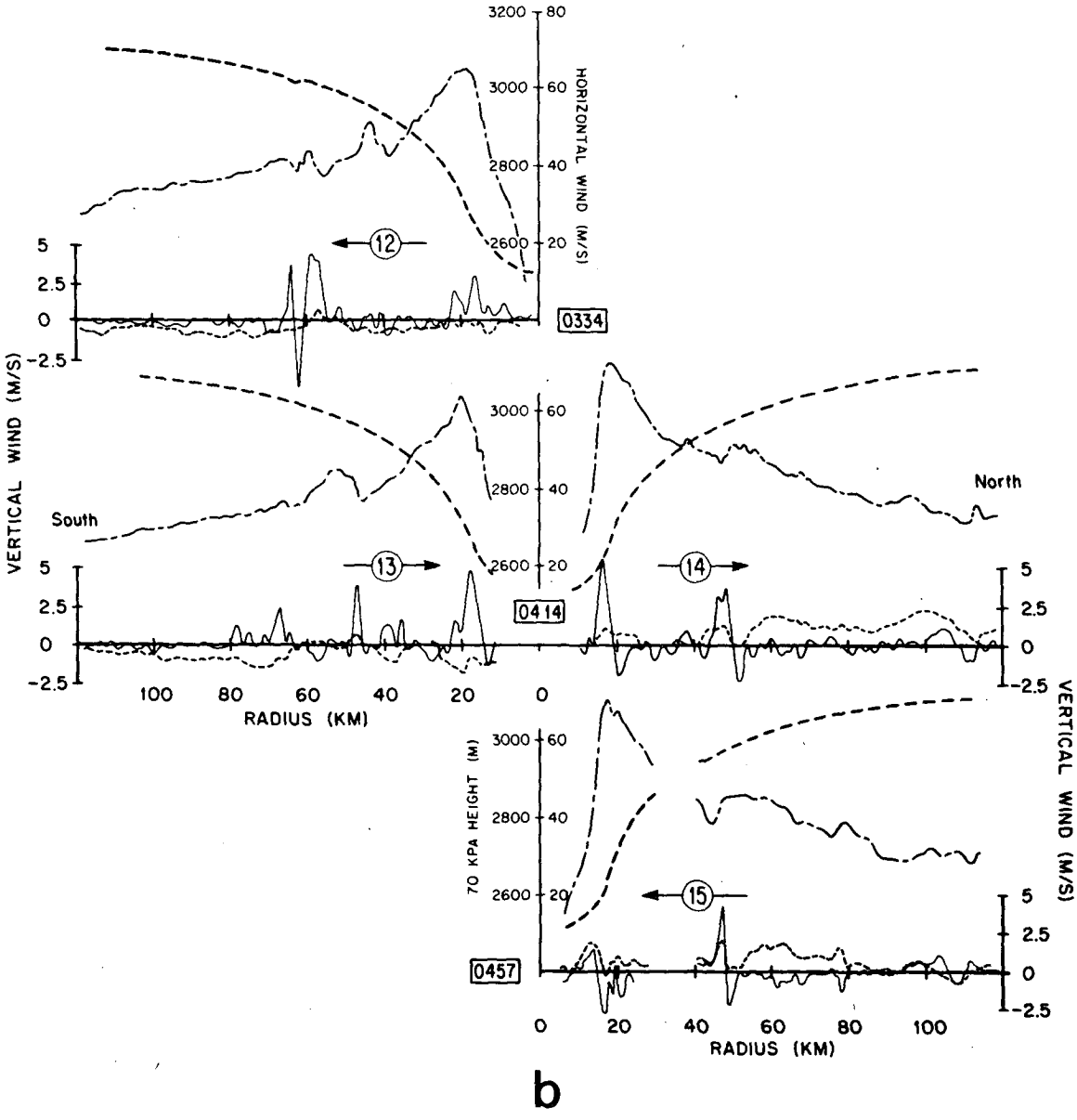

FIG. 2. (*Continued*)

that moves with the vortex center. Each profile is represented by 300 bins distributed along the 150 km maximum traverse length; however, some of the bins may be empty because of tape changes or data system failures. The value for each bin is a Bartlett average of the observations within 2 km of the bin's nominal radius. The interpolation program allows up to 16 radial traverses. Thus, all the values of a particular variable measured during a single aircraft sortie are represented as an array that contains a maximum of 16 × 300 elements. The first index denotes the traverse and the second the bin.

With the data in this form, the regression algorithm is run for all the bins at each radius in turn. If the bins at a given radius have missing data for three or more of the traverses, the algorithm is not executed. When the regression line is determined for each radius, it represents an estimate of the azimuthal mean variable as a function of time at the fixed radius. The effects of asymmetric transients as well as higher-order time variations in the symmetric structure are cast into the rms error that remains after the estimate is determined. The more permanent wavenumber 1 asymmetry is not confounded with the time variation of the symmetric vortex because the flight patterns were designed so that penetration of the vortex core from one side was immediately followed by an exit toward the opposite

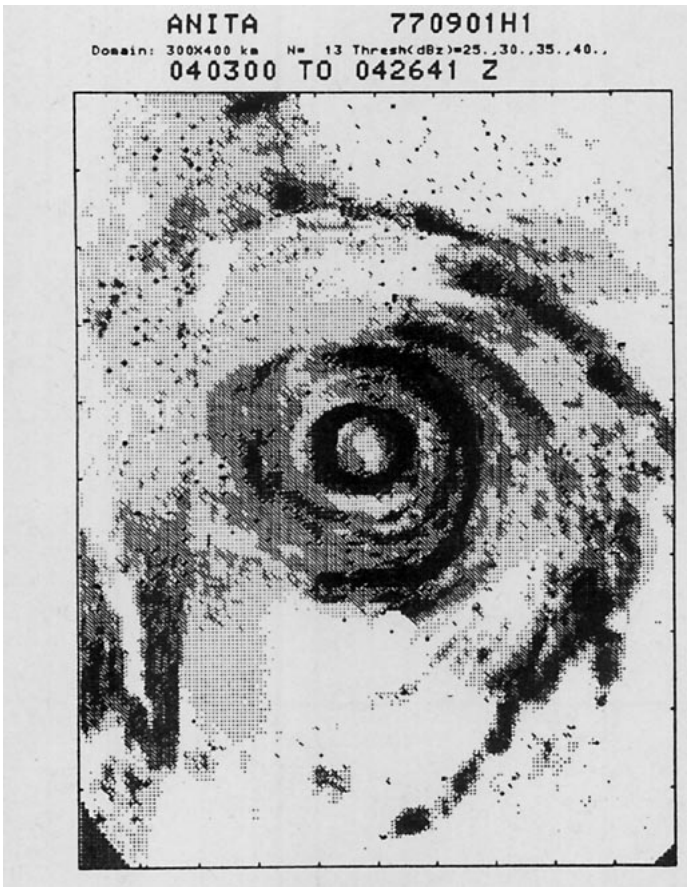

FIG. 3. Composite of digital radar reflectivity data observed in Hurricane Anita during passes 13 and 14 of Fig. 2b. Figure represents an area 300 × 400 km. (This and other radar imagery were prepared by Dave Jorgensen and Frank Marks of NHRL.)

side, and the traverses in any given direction were equally distributed about the center of the on-station period.

Fig. 8 illustrates the application of the foregoing analysis to the isobaric height and tangential wind data for Anita and David including an additional data set observed in David by NOAA-41 on 31 August 1979. For each aircraft sortie the estimated values are evaluated at the midpoint of the aircraft on-station time. The change is the product of the slope of the linear estimate and the aircraft's duration in the storm. For comparison we also show the rms error remaining after the estimate is determined. Generally, the *t*-test indicates that the slopes are significantly different from zero at the 5% level except where they cross the axis.

We concentrate first on the Anita data, which represents 4.22 h of observations. The region of positive tangential wind tendency that extends outward from 50 km radius corresponds to the emerging secondary wind maximum in Fig. 2b. Little indication of this feature is present in the estimate evaluated at the middle of the onstation time because the secondary maximum had just begun to emerge then. A second region of positive wind tendency lies at and inside the eyewall and is a manifestation of the contraction and intensification of the eyewall wind maximum. As one would expect, the estimate for the symmetric tangential wind in Fig. 8a closely resembles profile 4 in Fig. 2a, and the sum of that estimate and half the tendency closely resembles profile 15 in Fig. 2b.

The 70 kPa height tendency in Fig. 8a is negative inside the eye and positive or essentially zero outside it. The regions in the eyewall and secondary maximum where the tangential wind is accelerating correspond to outward increases in the 70 kPa height tendency, just as one would expect from the gradient wind relation. Furthermore, the ring of decelerating tangential wind between the eye wall and secondary maximum has a reversed height tendency gradient. Since the two tendency curves arise from independent analyses of different observed quantities, their mutual consistency is gratifying.

Fig. 8b illustrates the tendencies calculated for observations in David on 30 August (Fig. 4). This data set contains only 10 radial traverses, so that the confidence levels and gradient wind consistency are reduced. The relationship between the tangential wind and its tendency supports the contraction of the outer maximum and weakening of the inner eye shown in Fig. 7 and has much firmer statistical support. The negative wind tendencies around the inner maximum and the positive ones at the outer are manifestations of this process and are statistically significant at the 5% level. As for Anita, the isobaric height tendency gradients agree with the wind tendencies. This is particularly true of the rapid rises inside the inner eye and the ring of falls between the two eyewalls.

The final set of observations in Fig. 8c are the result of NOAA-41's flight in David on 31 August 1979. This data set comprises only eight profiles so that the statistical significance and gradient balance consistency are weaker. Only a single eye wall was evident on radar (not shown). The wind tendencies exhibit a pronounced, statistically significant peak just inside the radius of maximum wind. Clearly, the eye is contracting and the maximum wind increasing. This feature is sustained by a positive height tendency gradient. The reversed gradient just outside the eye, however, is not associated with a deceleration. Generally, the wind and pressure-height tendencies outside the eye are not statistically significant. Despite this limitation in the outer vortex, the character of the eyewall's evolution is clearly the same as Anita's eyewall in terms of the location and prominence of the strongest wind increase.

3. Typhoon data

Tropical cyclone reconnaissance reports constitute an additional source of data that relates evolution of concentric eyewalls to intensity changes. Central

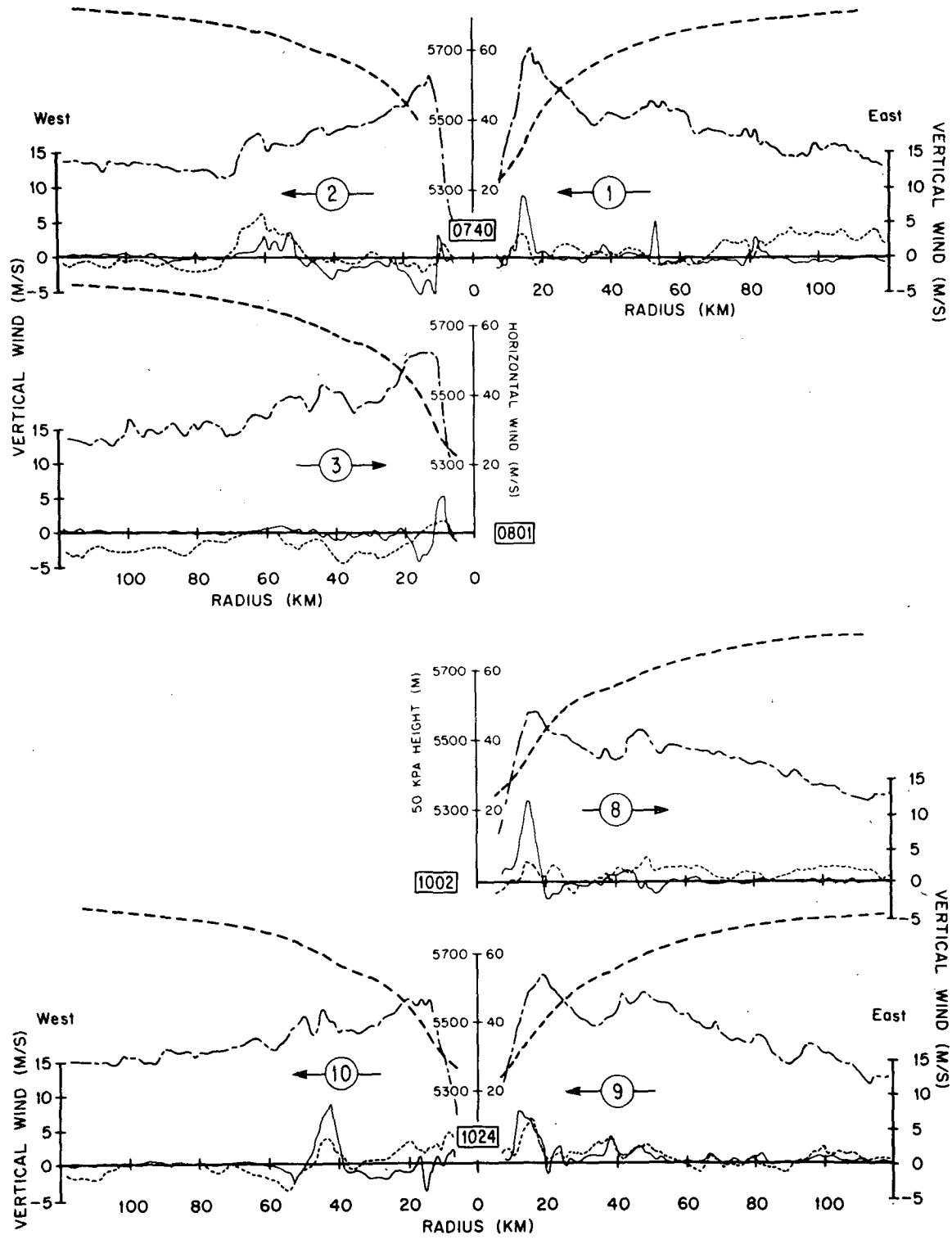

FIG. 4. Radial profiles observed in Hurricane David on 30 August 1979. These plots follow the same format as Fig. 2.

sea level pressure, eye diameter, and eye character (circular, elliptical, concentric) are routinely reported by operational reconnaissance aircraft. Indeed, Fig. 1 is based on such data. The reports for Pacific typhoons are presented in a particularly accessible form in the Joint Typhoon Warning Center's (1969–1971) *Annual Typhoon Report*. This section treats data observed in the Pacific during 1969–1971.

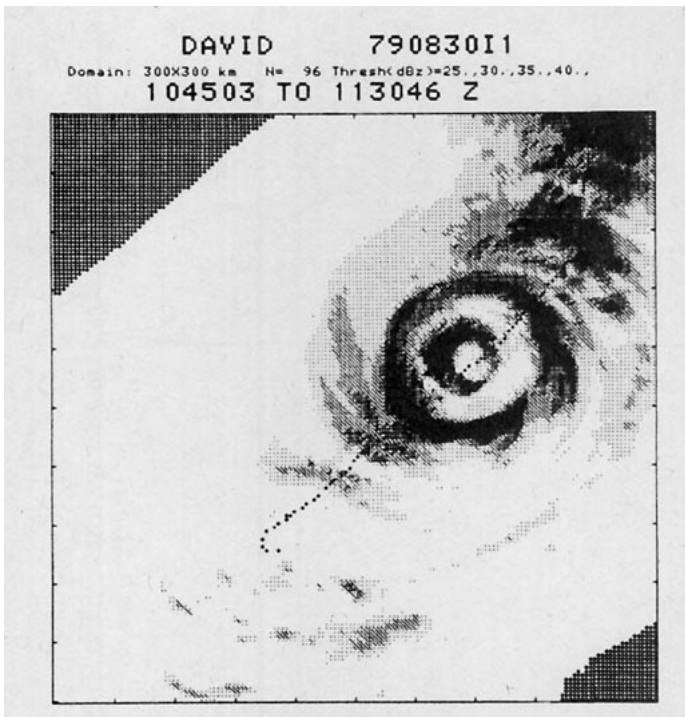

FIG. 5. Composite of digital radar reflectivity data obtained in Hurricane David during the hour after the latest data in Fig. 4 were collected. The plus signs indicate the aircraft track, and the frame represents an area 300 km square.

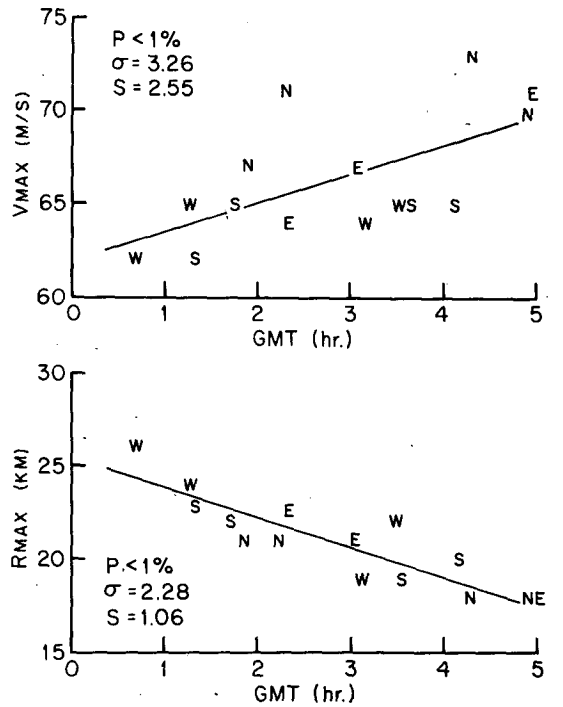

FIG. 6. Linear least-squares fits to the maximum wind and radius of maximum wind for all the profiles in Hurricane Anita. The letters denote observed values and their directions from the storm center. P is the significance with which the slope differed from zero, σ the rms departure from the mean, and S the rms departure from the linear estimate.

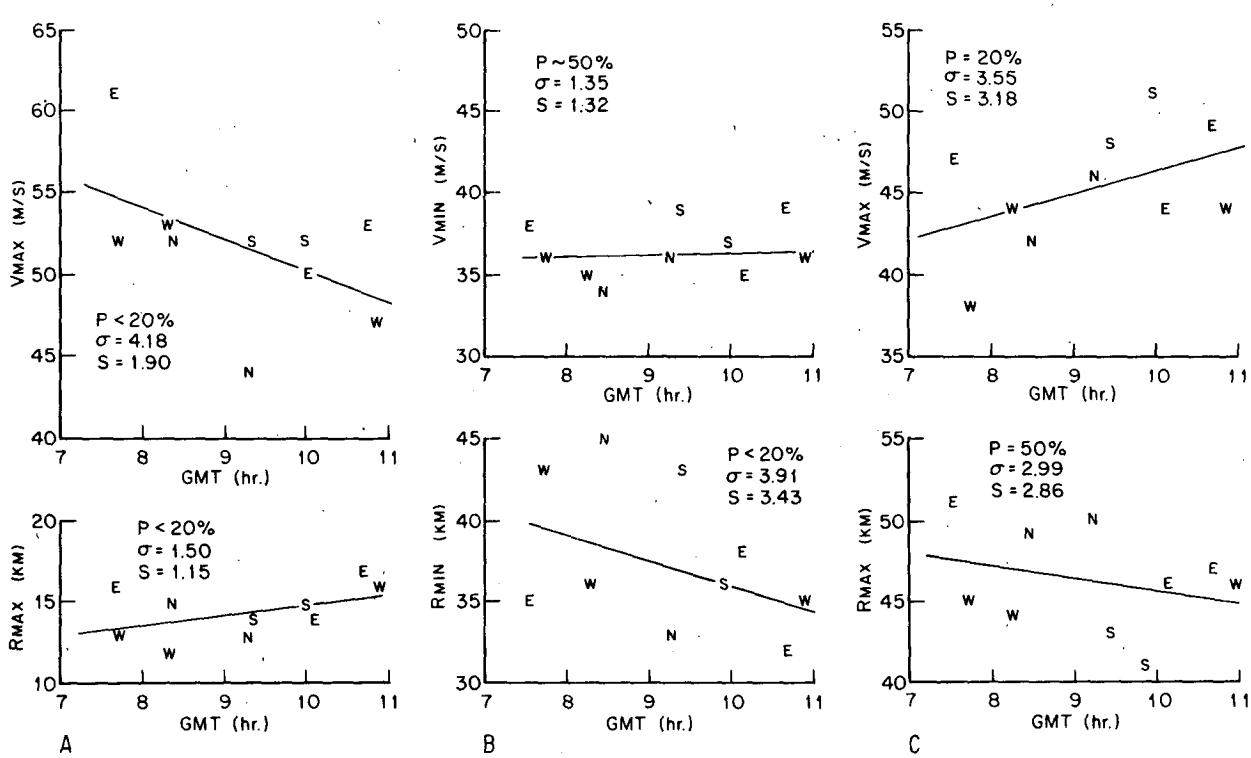

FIG. 7. As in Fig. 6, but for Hurricane David on 30 August 1979. These data represent (A) the inner eye wind maximum, (B) the minimum between the maxima, and (C) the outer maximum.

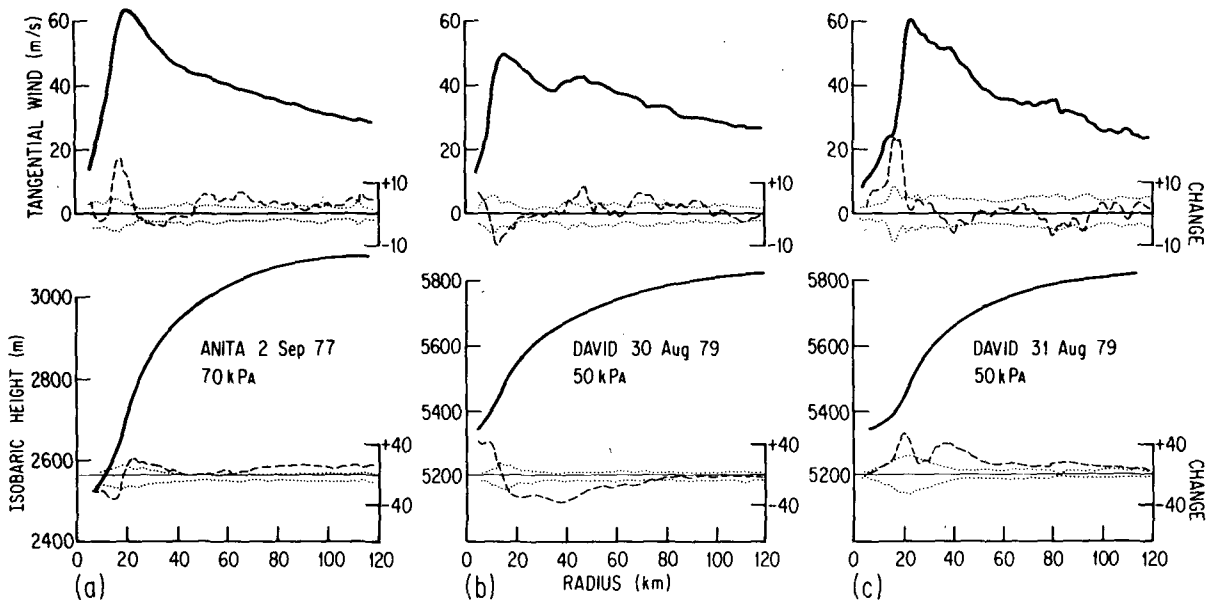

FIG. 8. Radial profiles of the estimated values (solid lines), tendencies (dashed lines), and rms error (dotted lines) for the tangential wind (upper panels) and isobaric height. Valid times and durations are: (a) Anita, 0251 GMT, 2 September 1977, 4.22 h; (b) David, 0925 GMT, 30 August 1979, 3.50 h; (c) David, 0823 GMT, 31 August 1979, 2.38 h.

We choose these years because before 1969 concentric eyes were not commonly noted, and after 1971 the naval WC-121 aircraft equipped with APS-20, 10 cm wavelength search radar was no longer available.

Table 1 summarizes the reported occurrences of concentric eyes during the three years in question. It must be emphasized that it is probably an underestimate of the actual number. This is particularly true for the single case reported in 1969. The senior author was assigned to the naval reconnaissance squadron in 1970 and 1971 and recalls that post-analysis of radar films occasionally revealed concentric eyes that had not been reported in the operational vortex messages.

Despite this limitation, we are able to establish that concentric eyes become more common with increasing intensity. Roughly half the supertyphoons ($v_{max} > 65$ m s^{-1}) exhibited concentric eyes, whereas such features appeared in only 1/10 of typhoons with $v_{max} < 65$ m s^{-1} and in none of the tropical storms ($v_{max} < 33$ m s^{-1}).

Variations in intensity were frequently associated with concentric eyes. Fig. 9 illustrates the history of eye diameter and central pressure for 5 of the cases that compose Table 1. In each of these the appearance of the concentric eye marks the end of a deepening phase, but does not necessarily indicate a weakening. The pressure may remain constant for a time before deepening resumes. This correlation is consistent with the cases cited in Section 1, as well as with Hurricanes Anita and David. Nevertheless, some caution should be employed in using this as a forecast rule. The concentric eyes were usually reported after peak intensity occurred. All of these cases were dramatic enough to impress observers who were not looking for them, and the concentric eyes had probably been present for a time before they were reported. Less spectacular occurrences that completely escaped the observers' attention may not have been so well correlated with cessation of deepening.

4. Hurricane Allen

By midsummer 1980 we appreciated the similarity between the SW model and the observations in David and Anita. In a sense the work done before 5 August 1980 might be regarded as the exploratory phase of the investigation, and the subsequent observations in Hurricane Allen as the confirmatory phase.

The early development of Allen was similar to David's. Both were Cape Verde storms, both entered the Caribbean as intense hurricanes, and, as Figs.

TABLE 1. The occurrence in the western Pacific of concentric eyes in tropical storms (TS, $v_{max} < 33$ m s^{-1}), typhoons (TY, $v_{max} > 33$ m s^{-1}), super typhoons (STY, $v_{max} > 65$ m s^{-1}) and typhoons excluding super typhoons (TY − STY) for the years 1969–71. The format is number of concentric eyes/number of storms.

Year	TS	TY	STY	TY − STY
1969	0/06	1/13	0/02	1/01
1970	0/12	5/12	3/07	2/05
1971	0/11	5/24	5/06	0/18
Total	0/29	11/49	8/15	3/34

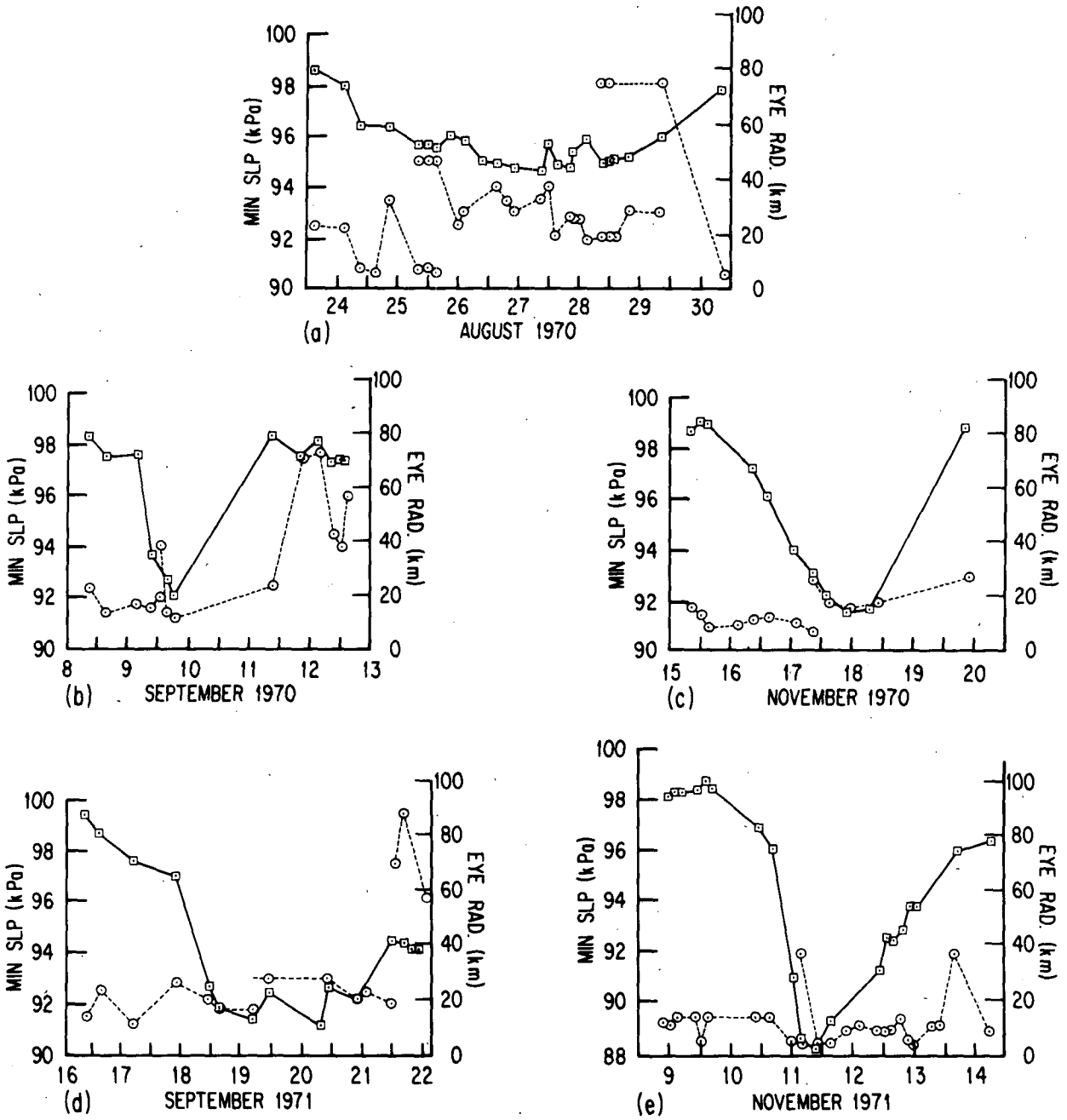

FIG. 9. Evolution of eye radius (dashed lines) and central pressure (solid lines) for Western Pacific typhoons Billie (a), Georgia (b), Patsy (c), Bess (d) and Irma (e).

1b and 10 show, both underwent cycles of intensification and weakening associated with fluctuations in the diameter of the eye. David was disrupted by passage over the Greater Antilles, but Allen continued south of the islands on a westward course that led through the Yucatan Channel to eventual landfall on the Texas coast (Lawrence and Pelissier, 1981).

The confirmatory data set comprises two 3-aircraft missions and one single-aircraft mission. The first multiple-aircraft mission was flown on 5 August 1980 as an intensifying, outer convective ring was replacing a dissipating relict inner eye. The second was flown on 8 August 1980 as the storm was rapidly deepening. The single-sortie mission on the next day investigated the weakening eye wall and outer maximum as the storm made landfall. There were several other single-aircraft missions, but they, as well as

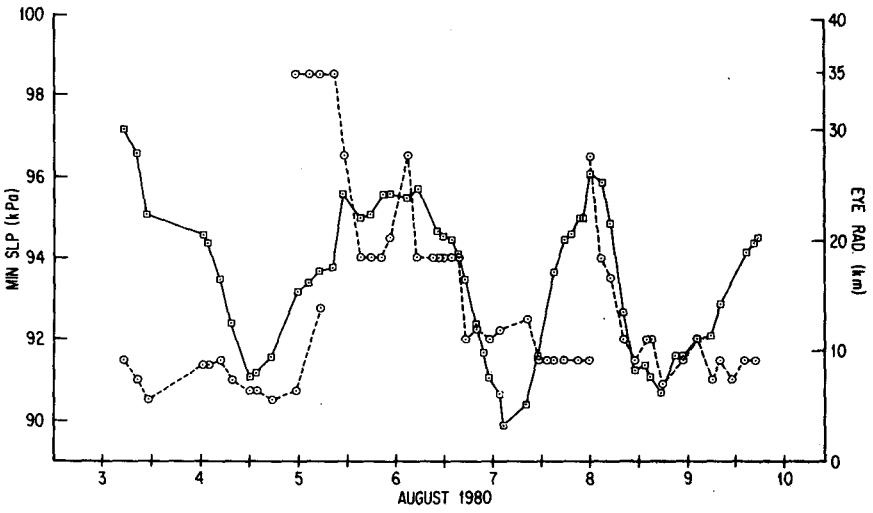

FIG. 10. Evolution of eye radius and central pressure for Hurricane Allen.

one of the sorties from 5 August, were unsuitable for statistical analysis because their flight patterns did not cover the vortex core symmetrically.

Fig. 10 shows that, before 5 August, Allen's eye had remained <10 km in radius for two days. When the research aircraft arrived at the storm, the radar, as shown in Fig. 11, revealed a dissipating relict inner eye surrounded by a 40 km radius outer maximum. (Fig. 17d shows this feature in a single radial profile of the tangential wind.) Clearly, the outer wind maximum was the primary eye wall, and the inner maximum was associated with the crescent-shaped hub cloud near the vortex center in Fig. 10. The relict wind maximum and hub cloud dissipated during the course of the mission.

Although the flight patterns were designed to facilitate study of convective features northwest of the center, two of them were symmetric enough to permit estimation of the structure and evolution of the tangential wind and isobaric height fields. These are shown in Fig. 12. The qualitative features of both the tendencies and the mean structure have much in common with Fig. 8b. Plainly, the destruction of the inner eye has progressed further in this case. Indeed, the relict wind maximum disappeared so quickly that the only hint of its presence in the azimuthal mean is a slight flattening of the wind profile near 20 km radius. Both the weakening of the tangential wind in the relict eye and its strengthening inside the outer eye wall are supported by appropriate gradients of pressure height tendency. In all, this is another example of the sequence of events that the SW model suggests for an outer maximum's transformation into the primary eye wall.

On 8 August 1980, the data were of substantially better quality. This mission was specifically designed to investigate the structure and evolution of the vortex core at three different lower tropospheric levels. The only disappointment involved early departure of the uppermost aircraft due to lightning damage. Otherwise the flight operations were ideal.

During the course of the mission the storm deep-

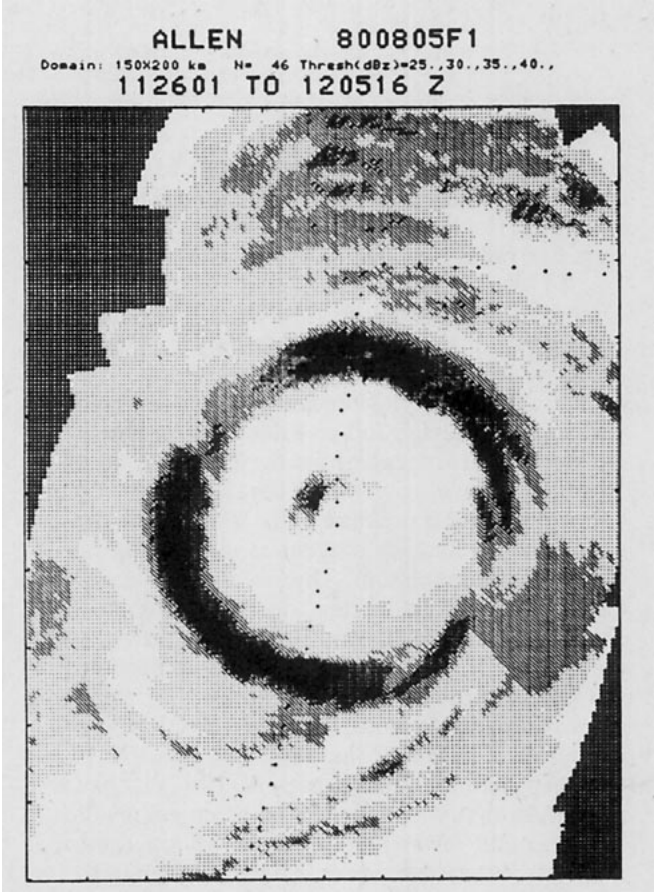

FIG. 11. Composite of digital radar reflectivity data observed in Hurricane Allen on 5 August 1980. Figure covers an area 150 by 200 km.

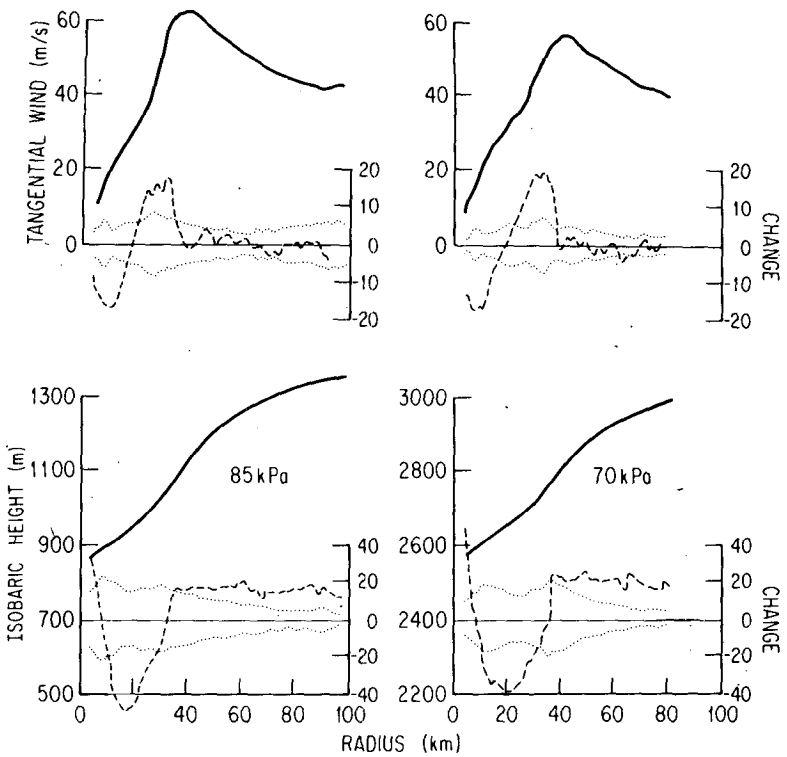

FIG. 12. As in Fig. 8 except for two of the three sorties flown on 5 August 1980. Both sets of estimates are valid at 1444 GMT, and the changes are standardized to represent a 6 h duration.

ened rapidly and the eye contracted. Fig. 13 illustrates the storm's appearance on radar. The eyewall is isolated from the outer wind maximum associated with the radar returns 120 km east of the center. Fig. 14 shows the estimates and tendencies of the azimuthal mean structure. The outer maximum does not appear in the estimates; its only manifestation is increased residual rms error at 120 km. This appears to have happened because the outer maximum was asymmetric and some of the radial traverses did not extend far enough from the center to reach it. At all three levels the vortex core exhibits the same pattern of strong pressure falls confined to the eye and rapidly increasing tangential wind just inside the eyewall wind maximum. The isolated eye and dense data coverage in the vortex core make this case suitable for a number of quantitative comparisons with the SW model. These are presented in Section 5.

The final mission in Allen was flown on 9 August as the storm made landfall. One of the observed tangential wind profiles from this sortie, Fig. 17b, shows that an outer maximum is present. If this is the same maximum that was observed on the previous day, it has migrated inward from 130 to 80 km radius. It also has become more pronounced relative to the inner eye. This is due largely to weakening of the wind in both the vortex core and the saddle between the two maxima. During the early part of the flight the outer maximum intensified and migrated inward to such an extent that its evolution was apparent in real time aboard the aircraft. Later, as its western extremity made landfall, it began to weaken and the wind in the saddle increased. Throughout the flight, the inner wind maximum weakened and expanded. This qualitative description agrees with the results of the statistical tendency calculation, shown in Fig. 15. The outer maximum's cycle of intensification and weakening appears as increased residual rms error between 70 and 100 km. This is because the intensification and weakening largely canceled, so that the net change is nearly zero over the flight's duration.

5. Quantitative comparison with the SW model

The SW model diagnoses the secondary circulation induced by point sources of heat or momentum in specified, hurricane-like, barotropic or baroclinic vortices that are in gradient and hydrostatic balance. SW present solutions for the streamfunction in the radius–height plane accompanied by the induced tendencies of isobaric height and tangential wind for a variety of vortex intensities and source locations. Over a wide range of these parameters the pattern of tendencies is much the same. Within the eye the isobaric height falls rapidly; outside the eye it falls more slowly. This leads to a sharp gradient of height

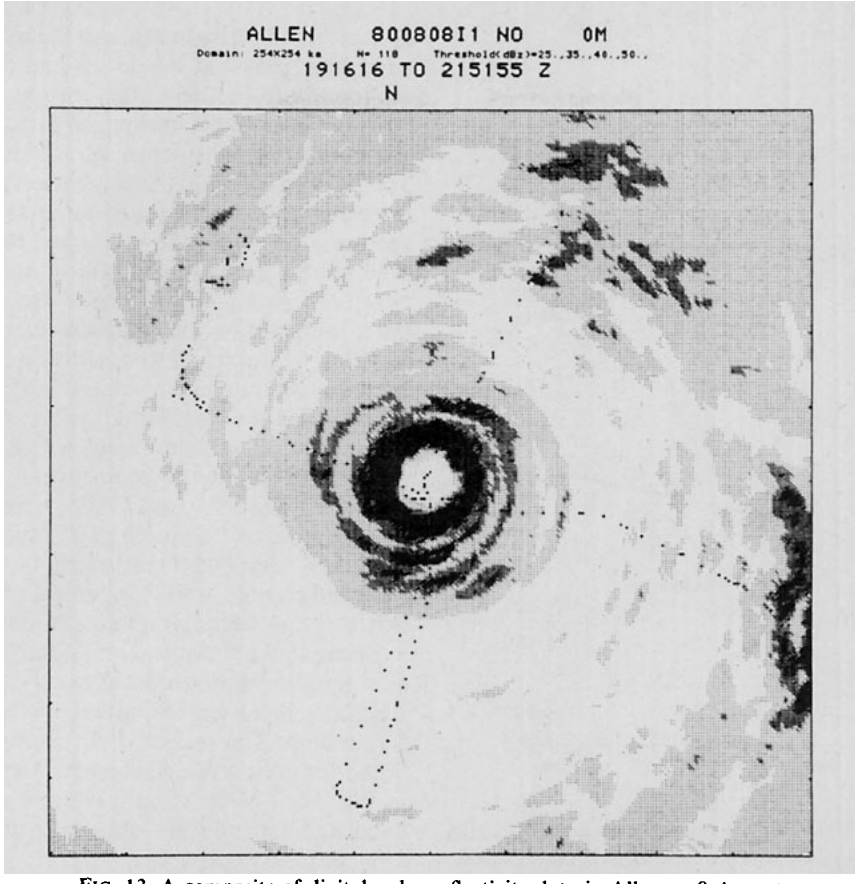

FIG. 13. A composite of digital radar reflectivity data in Allen on 8 August 1980. The linear dimensions of the area shown here are 254 km × 254 km.

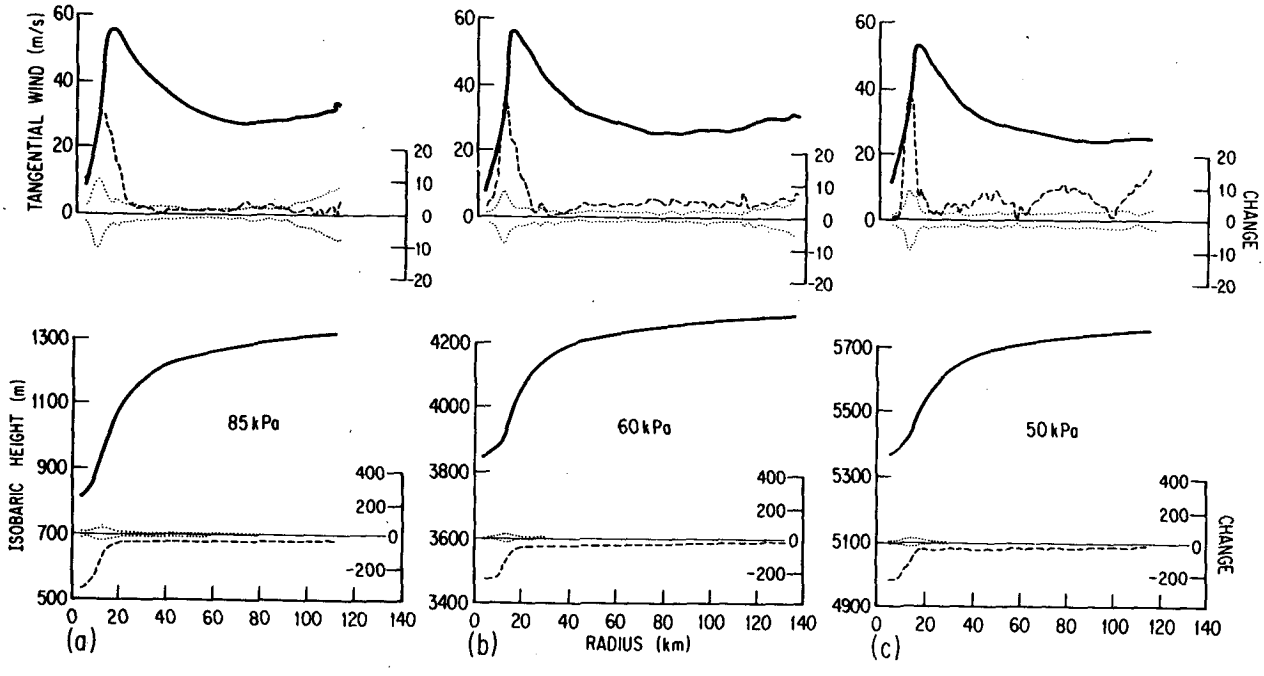

FIG. 14. As in Fig. 8 except for the 3-aircraft mission on 8 August 1980. All the estimates are valid at 2030 GMT, and the changes represent a 6 h duration.

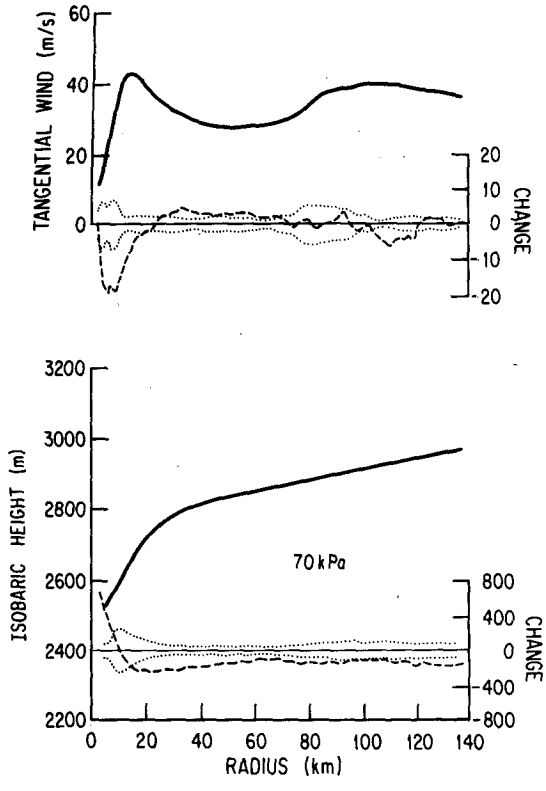

FIG. 15. As in Fig. 8 except for the single-sortie mission in Allen on 9 August 1980. The estimates are valid at 2031 GMT, and the changes represent 4.52 h duration.

tendency at and just within the wind maximum. Because of the gradient wind relation, the tangential wind tendency exhibits a sharp peak where the gradient of height tendency is strongest. The foregoing features are in qualitative agreement with the observations in Figs. 8, 12, 14 and 15.

Both theory and observations locate the maximum wind increase on the inward side of the maximum of the wind itself. This is crucial to the connection between the SW model and the concentric eye cycle because the SW model can thus provide a plausible physical explanation for the contraction of the outer wind maximum.

Some further discussion of the physics of the SW model is appropriate. The strong gradient of isobaric height tendency and the peak in the wind tendency arise from the radial change of the character of the secondary circulation near the eyewall. Outside the eye, the inertial resistance to horizontal motion (i.e., the horizontal gradient of angular momentum) is weak compared to the thermal stratification. The motions there involve radial flows that redistribute momentum effectively but do not readily change the mass field. Within the eye the inertial resistance and thermal stratification become comparable. The motions inside the eye have substantial vertical components and redistribute mass effectively. Thus, the updraft induced by heating in the eyewall has largely horizontal inflow at low levels and largely horizontal outflow aloft in the outer vortex. Within the eye, however, horizontal motions are restricted so that the compensating subsidence occurs near the updraft. The peak in the winds' acceleration may be explained in terms of either intense angular momentum advection when the inflow reaches the vortex core or the induced gradient of isobaric height tendency between the strong subsidence warming in the eye and the largely horizontal motions outside it. SW choose to think in terms of momentum advection and to evaluate the tendencies at the surface, so that their changes in the tangential wind arise from radial momentum advection alone. Away from the surface vertical advection of momentum becomes equally important. On 8 August 1980 the observed azimuthal mean updraft of about 2 m s^{-1} and a vertical shear of 1 m s^{-1} km^{-1} are sufficient to explain the total observed change in the tangential wind at the updraft axis through vertical advection alone.

Because the 8 August mission observed the effect of a single isolated convective ring, we attempt to simulate the observed pattern of tendencies with the SW model. The specified vortex structure and computed induced tendencies at 3.75 km altitude appear in Fig. 16. The maximum wind, radius of maximum wind and latitude are chosen to be the same as in

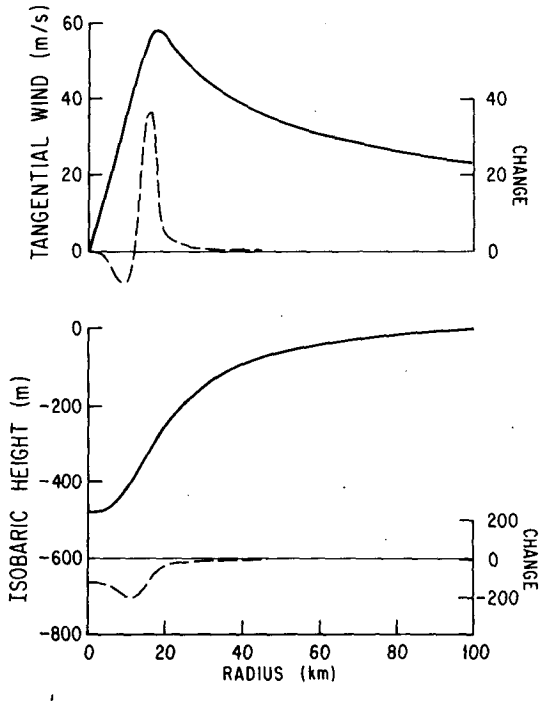

FIG. 16. Tangential wind and isobaric height anomaly tendencies calculated from the SW model. These are evaluated at 3.75 km altitude for a vortex and heat source scaled to represent Hurricane Allen on 8 August 1980. They are most directly comparable to Fig. 14b.

TABLE 2. Calculated and observed properties of Hurricane Allen on 8 August 1980.

Pressure (kPa)	r_{max} (km)	v_{max} (m s^{-1})	$(v_g)_{max}$ (m s^{-1})	$\left(\frac{\partial v}{\partial t}\right)_{max}$ [m s^{-1} (6 h^{-1})]	$\overline{\frac{\partial v}{\partial t}}$ [m s^{-1} (6 h^{-1})]	$\overline{\frac{\partial v_g}{\partial t}}$ [m s^{-1} (6 h^{-1})]	Δr_{max} [km (12 h^{-1})]
50	17.0	53.5	55.0	37.7	16.5	23.6	−18.2
60	15.0	57.1	55.6	36.2	17.2	15.8	−7.6
85	16.0	56.6	55.6	30.1	22.5	23.4	−7.4
Average	16 ± 1.0	55.7 ± 2.0	55.7 ± 0.8	34.7 ± 4.0	18.7 ± 3.3	20.9 ± 4.4	−11.1 ± 6.2

Fig. 14b. The altitude at which the tendencies are computed is as close to that in Fig. 14b as the finite difference scheme of the model allows. The heat source extends radially from 9 to 19.8 km and vertically from 500 m to the tropopause at 15 km. The heating rate in this volume was adjusted to give a simulated azimuthal mean updraft of 2.4 m s^{-1} at 13.6 km radius compared with the observed maximum azimuthal mean of 2.3 m s^{-1} at 13.5 km. The value of the average heating rate required to produce this updraft was 55°C day^{-1}, equivalent to a rainfall rate of 225 mm day^{-1} or a radar reflectivity of 38 dBZ.

The irregular pattern of positive wind tendencies and the uniform pressure fall in the outer vortex shown in Fig. 14 are not associated with the convective ring in the eye wall and are not simulated. If we concentrate on the vortex core, the primary difference between the model results and observations is the region of negative tangential wind tendencies in the center of the vortex. This feature appears in other observational cases (Figs. 8a, 8b and 12) and could be eliminated by judicious adjustment of the geometry of the heat source in the simulation. It also is true that the peak wind increase in the model is narrower than in Fig. 14b, but this also could be rectified by tuning the heat source. The confirmatory nature of the calculation lies in the fourfold agreement between the model and observations: magnitude of the maximum updraft, magnitude of the maximum wind increase, location of the peak wind increase, and magnitude of the maximum pressure fall. Only the first of these was adjusted to match the observations; the others follow from the model.

Given the quality of the data and the simple, isolated convective ring in the eye wall on 8 August, several more quantitative checks are possible. The first such is a check for gradient balance in the eye wall:

$$(v_g)_{max} = \left[g r_{max} \left(\frac{\Delta z_p}{\Delta r} \right) + \frac{f^2 r_{max}^2}{4} \right]^{1/2} - \frac{f r_{max}}{2}, \quad (1)$$

where g is the gravitational acceleration, f the Coriolis parameter, and Δz_p the increment of isobaric height across a 4 km interval Δr centered on r_{max}. A second check involves comparison of the tangential wind's maximum and average tendencies, $(\partial v/\partial t)_{max}$ and $\overline{(\partial v/\partial t)}$, with the gradient wind tendency approximated by

$$\frac{\partial v_g}{\partial t} = \frac{g\Delta\left(\frac{\partial z_p}{\partial t}\right)}{\xi \Delta r'}. \quad (2)$$

Here $\xi = 2v/r + f$ is the inertia parameter. The increment of pressure height fall, $\Delta(\partial z_p/\partial t)$, is taken over radial interval $\Delta r'$, equal to the width of the prominent wind tendency peak. $\overline{(\partial v/\partial t)}$ also is calculated over $\Delta r'$. This, of course, is not the rate at which the maximum wind is increasing because the maximum wind and maximum tendency do not coincide. The acceleration in (2) contributes more to the eyewall's contraction than to its intensification. Finally, a variation of Pettersen's (1956) kinematic technique allows calculation of this rate of contraction of r_{max}:

$$c \equiv \frac{dr_{max}}{dt} = \frac{\left(\frac{\partial v}{\partial t}\right)_{max} - \left(\frac{dv}{dt}\right)_{r_{max}}}{\partial v/\partial r}, \quad (3)$$

where $(dv/dt)_{r_{max}}$ is the wind tendency at r_{max} and $\partial v/\partial r \approx v_{max}/r_{max}$ is the radial shear inside the eyewall.

The results of these calculations appear in Table 2. Comparison of v_{max} and $(v_g)_{max}$ indicates that the gradient wind relation is satisfied at r_{max}. This supports use of the balanced approximations in SW, although the exact agreement of both the values at 85 kPa and the means is fortuitous. It also implies that the secondary flow responsible for the observed tendencies does not arise from supergradient winds above the boundary layer. The computed gradient wind tendencies agree with the average observed tangential wind tendencies, but are about half the peak values. This happens because the tendencies were based on the change of geopotential fall across the total width of the wind tendency peak. Finally, Δr_{max} is the change in r_{max} computed from Δr_{max} = (12 h) × c. We compare this with the observed changes in eye diameter in Fig. 10. Between 1144 GMT on 8 August 1980 and 0021 GMT on 9 August, the inner radius of Allen's radar eye contracted from 28 to 11

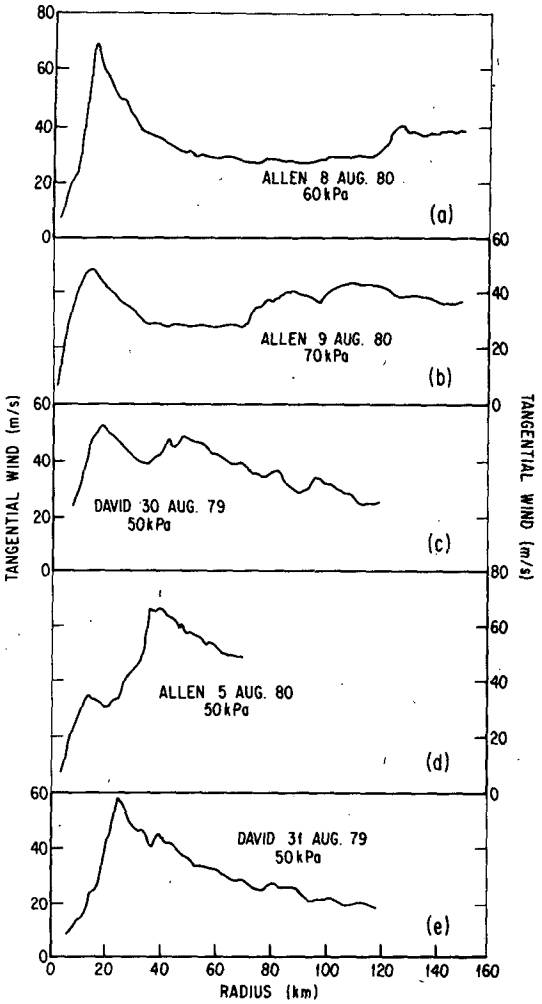

FIG. 17. An illustration of the concentric eye cycle made up from individual profiles in Hurricanes David and Allen.

km, equivalent to a change of 16 km $(12\ h)^{-1}$. Given that the inner radius of the radar eye and r_{max} are not identical (Shea and Gray, 1973), this is a satisfactory agreement with the average Δr_{max}, although the individual values have considerable scatter. Finally, r_{max} and v_{max} themselves show an interesting hint of vertical structure. The radius of maximum wind is smallest and the winds are strongest at 60 kPa. The eye expands and the winds weaken both above and below that level.

The consistency among the different flight levels in these two missions is gratifying. Even if the vertical variations in v_{max} and r_{max} in Table 2 represent real structure, one can obtain reliable indications of the evolution of the symmetric vortex with data from any lower tropospheric flight level above the boundary layer. Both the 85 kPa aircraft on 5 August and the 50 kPa aircraft on 8 August changed altitude by more than a kilometer during the course of their missions. Although the values in the last three columns of Table 2 for the 50 kPa sortie do not seem as reliable as those for the other two flights on 8 August, the qualitative interpretation is consistent.

6. Conclusions

We define convective rings as annular regions of active convective heat release that encircle the axes of tropical cyclones. This definition encompasses inner and outer concentric eye walls, but not spiral-shaped bands. Both earlier workers' results and the present observations support the following conclusions with regard to convective rings:

1) A persistent convective ring is often associated with a local tangential wind maximum.

2) If the ring contains active convective heating, the most rapid increase in windspeed lies on the inward side of the wind maximum. The maximum will thus contract as it intensifies. This, rather than a general increase in windspeed, appears to be the means by which symmetric hurricanes intensify. It also is the pattern of tendencies predicted by the diagnostic SW model.

3) Most convective rings force lower-tropospheric outflow and negative wind tendencies near the central axis of the vortex. When two concentric rings are present, this enables the outer to destroy the inner as it contracts about it.

4) The appearance of concentric rings is most common in intense hurricanes or typhoons, but it usually marks the end of an episode of intensification. Afterward, the storm may either weaken or maintain constant intensity for a time. Once the inner eye has completely dissipated, intensification may resume.

The foregoing conclusions are established only for symmetric convective rings. The dynamics of spiral-shaped disturbances and their influence on the vortex as a whole may be quite different.

Fig. 17 illustrates the concentric eye cycle using individual profiles from David and Allen. In this conceptual model, the outer convective ring forms more than 100 km from the center. Over a period of a day or two the ring constricts about the preexisting eye. When the outer ring's radius is two or three times that of the eye, the rings begin to interact, and the eyewall wind maximum weakens. In time, the outer eye predominates and encircles a relict wind maximum and hub cloud, which eventually dissipate.

The foregoing is not the only observed scenario. The outer maximum in Anita formed abruptly at between two and three times the radius of the original eye. Anita's maximum was also notably asymmetric; thus it may have formed by a different mechanism from the outer maximum in Allen.

Indeed, the mechanism by which convective rings initially form is unknown. Some possible mechanisms are: resonance between the local inertia period and asymmetric friction due to the storm's motion (Willoughby, 1979b), the action of precipitation-induced

downdrafts similar to those described in squall lines by Zipser (1977), or temporary symmetric instability (e.g., Bennetts and Hoskins, 1979) of the mean vortex. In the first mechanism, resonantly excited, radially propagating, asymmetric waves produce a convergence of the eddy momentum flux into their source region. This should force a radial outflow on the inward side of the wave source and thereby form a saddle in the wind profile. In the second mechanism the negative buoyancy due to precipitation falling from the overhanging cumulus anvil of the inner eye forces a downdraft surrounding the eye. Descent of low momentum air and low-level radial outflow induces a saddle in the wind profile. In the third mechanism symmetric instability arises from the small absolute vorticity and strong vertical shear at the base of the upper-tropospheric outflow layer. The instability will manifest itself as a ring of overturning air surrounding the center at 100–200 km radius. This would lead to moist convection that would become organized into a convective ring. Cumulus momentum transports would probably remove the symmetric instability once the ring had formed. For any of these mechanisms enhanced inertial resistance due to cyclonic shear inside the secondary wind maximum concentrates the boundary layer convergence, and hence the convection, into the ring. This convective ring then undergoes the cycle described by Fig. 17.

The concentric eye in Hurricane Debbie during the STORMFURY experiment remains a source of controversy. If it was a natural feature, it invalidates STORMFURY's apparent positive result; if it was caused by seeding, it represents a successful experiment. We have shown that something very like the hypothesized STORMFURY chain of events happens in unmodified hurricanes. The important question for hurricane modification is: Can the energy released by artificial manipulation of the cloud microphysics initiate or accelerate the formation of a convective ring? In any case, the documented relationship between the concentric eye cycle and intensity changes indicates that more careful attention to this phenomenon can contribute to improved intensity forecasts.

Acknowledgments. This study could not have been accomplished without the skill and professionalism of the RFC flight crews. Without diminishing the contributions of the others, we would like to thank individually the aircraft commanders: Jim Gunnoe, Howard Ticknor, Dave Turner, and Fred Werley; flight directors: Dick Darby, Harlan Davis, Jim McFadden, John Michie and Stig Rossby; and electronics engineers Jim Dugranrut and Terry Schricker. Several colleagues at NHRL contributed significantly to this study. Harry Hawkins and the late Billy M. Lewis planned the mission of 8 August; Dave Jorgensen and Frank Marks provided the radar imagery; and Marcy Chelmow and Jackie Piotrowicz contributed to the data processing. Discussions with them and especially with Lloyd Shapiro and Vic Ooyama also of NHRL and Ed Zipser of NCAR helped clarify our ideas. Suzanne Nole and Angel Tillman typed the manuscript, and Dale Martin drafted the figures. Their skill and patience are much appreciated.

REFERENCES

Bennetts, D. A., and B. J. Hoskins, 1979: Conditional symmetric instability—a possible explanation for frontal rainbands. *Quart. J. Roy. Meteor. Soc.*, **105,** 945–962.

Black, P. G., H. V. Senn and C. L. Coutright, 1972: Airborne radar observations of eye configuration changes, bright band distribution and precipitation tilt during the 1969 multiple seeding experiments in Hurricane Debbie. *Mon. Wea. Rev.*, **100,** 208–217.

Eliassen, A., 1951: Slow thermally or frictionally controlled meridional circulation in a circular vortex. *Astrophys. Norv.*, **5,** 19–60.

Fortner, L. E., 1958: Typhoon Sarah, 1956. *Bull. Amer. Meteor. Soc.*, **39,** 633–639.

Gentry, R. C., 1970: Hurricane Debbie modification experiments, August 1969. *Science,* **168,** 473–475.

Hawkins, H. F., 1971: Comparison of results of the Hurricane Debbie (1969) modification experiments with those from Rosenthal's numerical model simulation experiments. *Mon. Wea. Rev.*, **99,** 427–434.

Hebert, P. J., 1980: Atlantic Hurricane season of 1979. *Mon. Wea. Rev.*, **108,** 973–990.

Holliday, C. R., 1977: Double intensification of Typhoon Gloria, 1974. *Mon. Wea. Rev.*, **105,** 523–528.

Hoose, H. M., and J. A. Colón, 1970: Some aspects of the radar structure of Hurricane Beulah on September 9, 1967. *Mon. Wea. Rev.*, **98,** 529–533.

Joint Typhoon Warning Center, 1969–1971: *Annual Typhoon Report.* [NTIS AD 785178, AD 785252, AD 768333].

Jordan, C. L., 1966: Surface pressure variations at coastal stations during the period of irregular motion of Hurricane Carla of 1961. *Mon. Wea. Rev.*, **94,** 454–458.

——, and F. J. Schatzle, 1961: The "double eye" of Hurricane Donna. *Mon. Wea. Rev.*, **89,** 354–356.

Lawrence, M. B., 1978: Atlantic hurricane season of 1977. *Mon. Wea. Rev.*, **106,** 534–545.

——, and J. M. Pelissier, 1981: Atlantic hurricane season of 1980. *Mon. Wea. Rev.*, **109,** 1567–1582.

Pettersen, S. V., 1956: *Weather Analysis and Forecasting,* Vol. 1. McGraw-Hill, 428 pp.

Shapiro, L. J., and H. E. Willoughby, 1982: The response of balanced hurricanes to local sources of heat and momentum. *J. Atmos. Sci.*, **39,** 378–394.

Shea, D. J., and W. M. Gray, 1973: The hurricane's inner core region I. Symmetric and asymmetric structure. *J. Atmos. Sci.*, **30,** 1544–1564.

Willoughby, H. E., 1979a: Forced secondary circulations in hurricanes. *J. Geophys. Res.*, **84,** 3173–3183.

——, 1979b: Excitation of spiral bands in hurricanes by interaction between the symmetric mean vortex and a shearing environmental steering current. *J. Atmos. Sci.*, **36,** 1226–1235.

——, 1979c: Some aspects of the dynamics of Hurricane Anita of 1977. NOAA Tech. Memo. ERL NHEML-5, 30 pp. [Available from author.]

Zipser, E. J., 1977: Mesoscale and convective-scale downdrafts as distinct components of squall-line structure. *Mon. Wea. Rev.*, **105,** 1568–1589.